*Bulgarian Chemical Communications, Volume 48, Special Issue D (pp. 131 –137) 2016*

# Preparation, characterization and optical properties of nanostructured undoped and Cu doped ZnO thin films

Esmaeil Amaki, Reza Sahraei*

*Department of Chemistry, University of Ilam, P.O. Box: 65315-516, Ilam, Iran.*

Received June 26, 2016; Revised September 10, 2016

In this work, undoped and Cu-doped ZnO (ZnO:Cu) nanostructured thin films were synthesized by chemical bath deposition method. UV-Visible and photoluminescence (PL) spectroscopy have been used to investigation of optical properties of the samples in detail. The band gap energy of undoped and Cu-doped ZnO films is blue-shifted by ≈ 0.3 eV with respect to the bulk value (3.37 eV), probably due to the quantum size effect as expected from the nanocrystalline nature of the films. The photoluminescence (PL) spectra of the ZnO:Cu thin films exhibited two emission peaks, one blue peak located at 491 nm and a intense deep level-green peak at 521 nm. The intensity of photoluminescence emission is enhanced with increasing Cu concentration and deposition temperature. The intensity of peaks is optimized at Cu:Zn ratio of 0.29% for the ZnO:Cu thin films. Fourier transform infrared (FTIR) spectroscopy shows two peaks in 427.22 and 532.71 $cm^{-1}$ which is attributed to ZnO and CuO bonds, respectively. The x-ray diffraction and scanning electron microscopy techniques indicated that the films have hexagonal phase of ZnO.

**Keywords:** Nanostructures; Zinc oxide; Cu doped; Thin films; Optical properties

## INTRODUCTION

Zinc oxide (ZnO) with a wide band gap (3.37 eV) [1] and a large exciton binding energy of 60 meV [2] is one of the excellent semiconductors which can be applied to light emitting diodes, solar cells, and gas sensors [2-5]. Among metal oxides, ZnO has been studied intensively due to its rich optical properties. Besides, it can be prepared at a lower temperature. Owing to these properties, ZnO has attracted increasing attention as a promising candidate material for potential applications in optoelectronic devices [6-10]. The emission properties of undoped and doped ZnO films have been widely studied [11-13]. Recently, some researchers have found some doping elements, such as Ga, Ni, and Mg can influence the luminescence properties of ZnO films [14-16]. Copper is a prominent luminescence activator in II-VI compounds [17]. It is significant to investigate ZnO film doped with Cu for its possible luminescence application. The techniques used for ZnO growth include chemical vapour deposition (CVD), molecular beam expitaxy (MBE), Rf or dc sputtering, pulsed laser deposition (PLD) [18-20], and chemical bath deposition (CBD) [21-23], etc. Among these methods, chemical bath deposition is an attractive technique for obtaining thin films and has the advantage of easy control of the film composition and easy fabrication of large area thin film with low cost [24]. In this paper, we fabricated undoped and Cu-doped ZnO (ZnO:Cu) thin films on glass substrates through chemical bath deposition at range of 45-76 °C. The effect of fabrication conditions including the concentrations of Cu precursor and kinetic parameters (temperature and deposition time) on the structural, optical and photoluminescence properties of the ZnO:Cu thin films were investigated. The films are characterized by several techniques such as X-ray diffraction, scanning electron microscopy (SEM), UV-visible and fluorescence spectrophotometer.

## EXPERIMENTAL

Undoped and Cu-doped ZnO (denoted by ZnO:Cu) thin films were deposited on glass substrates by chemical bath deposition. The precursor materials used prepare undoped and doped ZnO films are zinc chloride ($ZnCl_2$), hexamethylentetramine ($C_6H_{12}N_4$), copper acetate monohydrate [$Cu(CH_3COO)_2.H_2O$] and ethanol (for seed layer of ZnO:Cu films, solutions of 0.1M $ZnCl_2$, in ethanol). Aqueous solutions of 0.1M $ZnCl_2$, and 0.1M $C_6H_{12}N_4$ with ratio 1:1 were mixed in a beaker for deposition undoped and Cu-doped ZnO thin films at 45-76 °C and deposition times of 1-8 h. In order to adjust the Cu concentration, the desired amounts of copper acetate solution were added ($5\times10^{-2}$–$5\times10^{-7}$ M and 1–10 mL).

The nanostructure and morphology of the films were studied by X-ray diffraction Xpert MPD with

* To whom all correspondence should be sent:
E-mail: reza_sahrai@yahoo.com

Cu Kα radiation (40 kV and 30 mA) and scanning electron microscope (SEM, S-4160 Hitachi), respectively. Photoluminescence (PL, Cary Eclips FL llll MO25) measurements were carried out at room temperature. The optical properties of the samplea were investigated by a UV-Visible (UV-Vis, Cary 300 Bio). Inductively coupled plasma atomic emission spectroscopy (ICP-AES, Varian Vista-Pro) confirmed the presence of copper atoms with different percentages as an impurity. Infrared spectrum was recorded on (FTIR, Vertex 70). Also, the thickness of the films was measured by thickness gauge needle (Dektak[3]).

## RESULTS AND DISCUSSION

### *X-ray diffraction (XRD)*

XRD patterns of the undoped and Cu-doped ZnO thin films prepared at 76 °C are presented in Fig. 1. It is apparent that four peaks can be designated to (100), (002), (101) and (102) planes of hexagonal wurtzite in ZnO thin films [25]. Fig. 1b shows double phase of ZnO:Cu and secondary phase can be detected, it is apparent that a (110) peak of monoclinic appears in ZnO:Cu thin films that correspond to copper oxide phase [26]. Fig. 1 shows, the intensity peaks ((100), (002), (101) and (102)) of ZnO:Cu decreased than to pure ZnO due to the presence of copper in the structure of ZnO can be attributed to changes in the make-up atoms. Also, It has happened angular shifting at the peak with adding copper, and according to Braggs rule, can be attributed change in atomic plates distance and layers compaction.

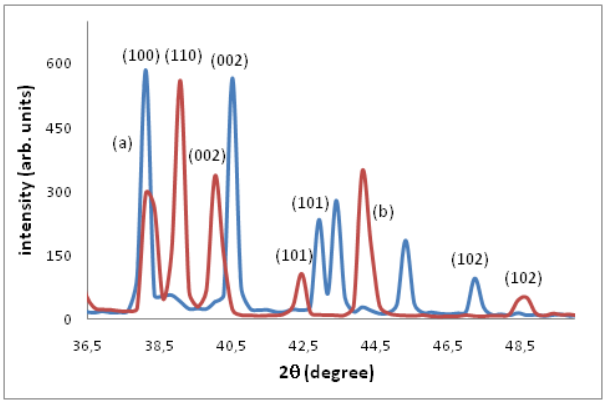


**Fig. 1.** XRD patterns of (a) ZnO (b) ZnO:Cu (Cu=0.5×10$^{-5}$ %) thin films.

Fig. 2 shows X-ray diffraction measurements on the Cu-doped ZnO films for different Cu concentrations, the peaks intensity hexagonal structure of ZnO decreased with increasing copper concentration, but the peak intensity increased corresponding Miller indices (110) monoclinic structure of CuO, that differences of intensities can be attributed to how to arrange of atoms in structure. XRD pattern of the Cu-doped ZnO thin films prepared at 56°C is presented in Fig. 3, and compared to Fig. 2a, the full width at half maximum (FWHM) of peaks is wider and indicates the smaller sized nanoparticles according to Braggs rule at 56 °C is formed. Also, the intensity of the (110) peak decreased which indicated that the dominant hexagonal phase is more stable than the monoclinic phase at 56°C.

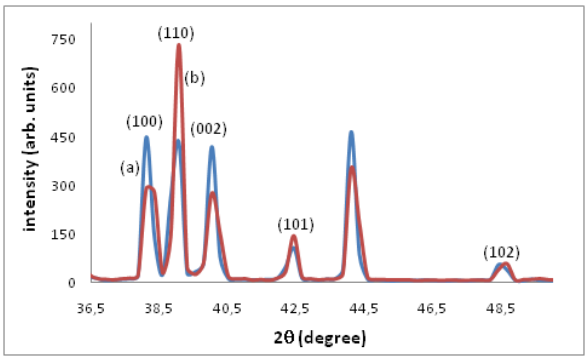


**Fig. 2.** XRD patterns of ZnO:Cu prepared at 76 °C (a) Cu=0.45×10$^{-4}$ % (b) Cu=0.03%

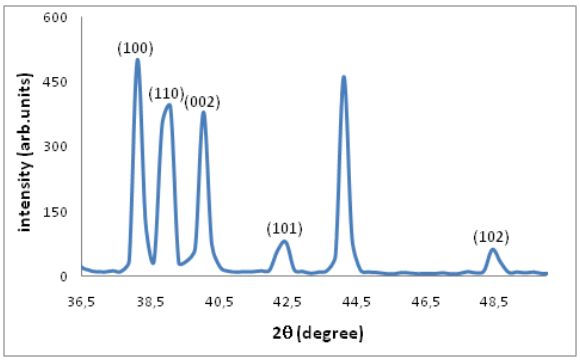


**Fig. 3.** XRD pattern of ZnO:Cu (Cu=0.45×10$^{-4}$ %) prepared at 56°C.

The broadening of peaks is related to small crystallite sizes and lattice strains:

$$B_r = B_{crystallite} + B_{strain} \quad (1)$$

The using Equation (2) for calculated $B_r$:

$$B_r = \sqrt{(B_0 - B_i)\sqrt{(B_0^2 - B_i^2)}} \quad (2)$$

Where, the remaining width $B_r$ is due to the combined effects of crystallite size and lattice strain, if the observed x-ray diffraction peak has a width $B_0$ and the width due to instrumental effects is $B_i$ ($B_i$=1.74×10$^{-3}$ rad).

The quantity $B_r\cos\theta$ can be plotted versus $\sin\theta$ according to Eq. (3):

$$B_r \cos\theta = \eta \sin\theta + \frac{K\lambda}{L} \quad (3)$$

Where $k$ is a constant ($k$=0.94), $\lambda$ is X-ray wavelength (CuKα ,$\lambda$=0.15406 nm), L is crystallite sizes. The plot of $B_r\cos\theta$ against $\sin\theta$, can be used to calculate from the intercept $K\lambda/L$ and the slope $\eta$ the crystallite size (L) and lattice strain (η), respectively [27, 28]. Fig. 4 and Fig. 5 shows plot of $B_r\cos\theta$ versus $\sin\theta$ for ZnO:Cu at 76 °C and 56 °C respectively. The values of lattice strain and crystallite size for ZnO:Cu thin films were shown in Table 1. The results shown, the full width at half maximum (FWHM) is more at 56 °C. Thus, the nanocrystal size is smaller and with lower lattice strains.

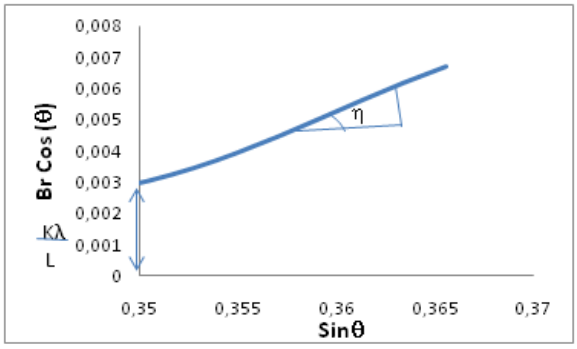


**Fig. 4.** Plot of $B_r\cos\theta$ versus $\sin\theta$ for ZnO:Cu (Cu=0.45×10$^{-4}$ %) at 76°C.

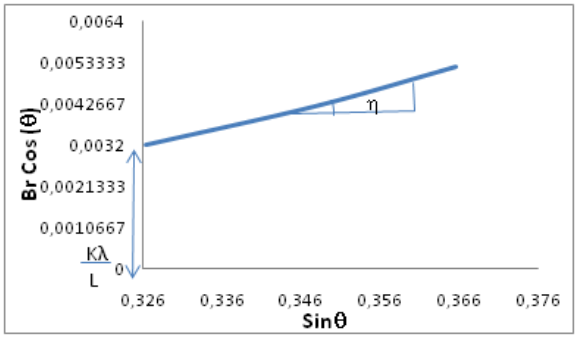


**Fig. 5.** Plot of $B_r\cos\theta$ versus $\sin\theta$ for ZnO:Cu (Cu=0.45×10$^{-4}$ %) at 56 °C.

**Table 1:** The values of lattice strains (η) and crystallite sizes (L) of ZnO:Cu

| Temperature (°C) | (η) | L (nm) |
|---|---|---|
| 56 | 0.0095 | 43.32 |
| 76 | 0.0101 | 46.21 |

*Surface morphology by scanning electron microscopy (SEM)*

The surface morphology of the undoped and Cu-doped ZnO thin film deposited on glass substrates at 56-76°C were studied by scanning electron microscope. Fig. 6 show the SEM images of ZnO thin film prepared at 76 °C. It exhibits a sheet like structure. Also SEM studies indicated that the product was hexagonal phase of ZnO thin film, which good agreement with the XRD results.

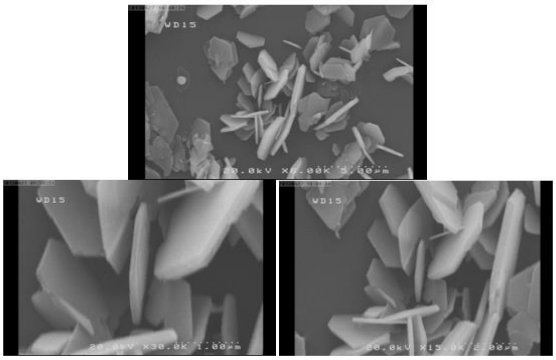

**Fig. 6.** SEM images of ZnO thin films.

In Figs. 7-8 the SEM images show ZnO:Cu thin film (seed layer). SEM studies indicated that the product was hexagonal and monoclinic phase attributed to ZnO and CuO respectively, which good agreement with the XRD results. Fig. 7 shows the SEM images of ZnO:Cu film deposited at 76 °C from different deposition times. The nanocrystal size increased with increasing deposition time. The size of ZnO:Cu nanocrystals due to seed layer is greater than ZnO pure (at the same time, compared with Fig.6), Also, after 8 hours deposition were completed hexagonal nanocrystals shown in the Fig. 7d. The photoluminescence peak intensities optimized with 0.45×10$^{-4}$ at % Cu doped ZnO at 76 °C (Fig. 7b).

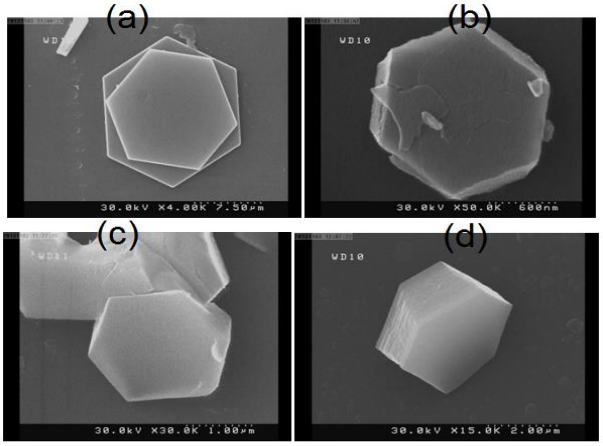


**Fig. 7.** SEM images of ZnO:Cu (Cu=0.45×10$^{-4}$ %) thin films prepared at different deposition times and at 76 °C (a) 1.5 h (b) 2.5 h (c) 4 h and (d) 8 h.

Fig. 8 show the SEM images of ZnO:Cu films deposited at 76 °C for different Cu doped. As can be seen, the images show that the monoclinic phase of copper oxide in comparison with Fig.7 is formed. Also, photoluminescence results show that increasing of copper concentration was decreased the intensity of emission due to electron capture by copper ions.

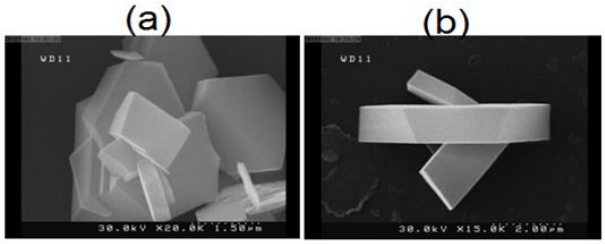


**Fig. 8.** SEM images of ZnO:Cu thin films prepared at different Cu concentrations and at 76°C for 4 h (a) Cu=0.004 % and (b) Cu=0.03 %

*Optical properties*

The energy gap of semiconductors represents fundamental physical aspects that characterize their optical and electronic properties. The optical energy ($E_g$) determines the threshold for absorption of photon in semiconductor. The energy gap of all the films is determined from the absorption coefficient (α) which can be calculated from the transmittance (T) of the ZnO thin films. The absorption coefficient (α) is calculated by the following formula:

$$\alpha = \frac{1}{d}\ln\frac{1}{T} \qquad (4)$$

where d is the film thickness. The absorption edge was analyzed by the following equation [29]:

$$(\alpha h\nu)^2 = A\,(h\nu - E_g) \qquad (5)$$

where A is a constant, $h\nu$ is the incident photon energy and $E_g$ is the optical band gap energy. Based on the Eq. (5) the plots of $(\alpha h\nu)^2$ as a function of incident photon energy $(h\nu)$ were obtained for the undoped and Cu-doped ZnO thin films and are shown Fig. 9, 10, and 11 indicate that the films are direct transition-type semiconductors. The linear portion is extrapolated to α=0, on energy axis, which corresponds to the $E_g$ undoped and Cu-doped ZnO thin films shown in Table 2. Kinetic parameters (temperature and time deposition) are influenced on the band gap energy, where with increasing temperature and deposition time the band gap energy of films is decreased.

Brus for the first time considered the correction of exciton energy and energy of the quantum confinement in the Schrödinger wave equation. So using equation (6) one can calculate the radius (R) of the ZnO nanocrystals using following equation [30-32]:

$$E_g^{NC} = E_g^B + \frac{h^2}{8R^2}\left(\frac{1}{m_e} + \frac{1}{m_h}\right) - \frac{1.8e^2}{4\pi\varepsilon R} \qquad (6)$$

where $E_g^{NC}$ is band gap energy of nanocrystas, $E_g^B$ is band gap energy of the bulk, h is Planck constant, $e$ is electric charge of electron, ε is relative dielectric constant (ε=8.66 for wurtzite ZnO), $m_e$ and $m_h$ is electron effective mass and hole effective mass respectively ($m_e$=0.28$m_0$ and $m_h$=0.78$m_0$ for wurtzite ZnO), $m_0$ is the electron mass at rest [33-35]. The nanocrystals radiuses for undoped and Cu-doped ZnO thin films are shown in Table 2. With increasing deposition kinetic parameters, the nanocrystals radius of the undoped and Cu-doped ZnO thin films increased due to quantum effects.

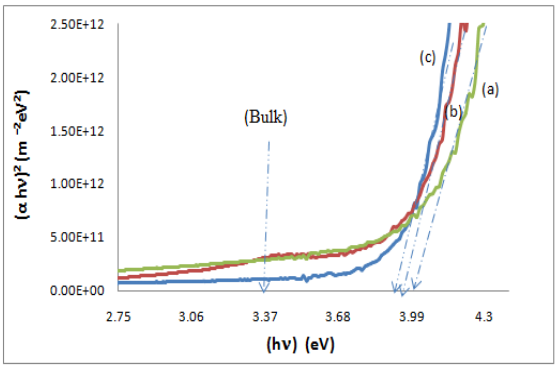


**Fig. 9** Plot of $(\alpha h\nu)^2$ versus hν for the ZnO thin films prepared at 60°C and at different deposited times (a) 3 (b) 6 (c) 8 h.

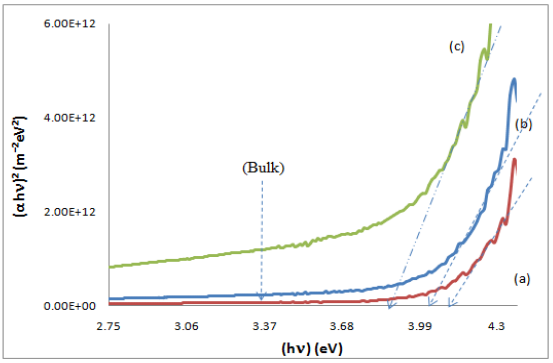


**Fig. 10** Plot of $(\alpha h\nu)^2$ versus hν for the ZnO thin films prepared at different deposition temperatures (a) 45 (b) 60 (c) 76 °C.

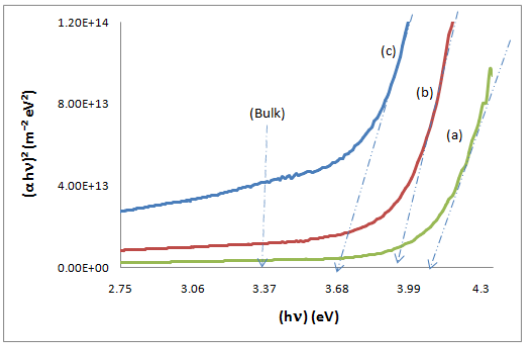


**Fig. 11** Plot of $(\alpha h\nu)^2$ versus hν for the ZnO:Cu thin films prepared at 76 °C and at different deposited times (a) 1.5 (b) 3 (c) 4h.

## PHOTOLUMINESCENCE STUDIES

Fig. 12 shows the photoluminescence (PL) spectra of the undoped and Cu-doped ZnO prepared at various Cu concentrations and at 76°C. The PL measurements were performed at excitation wavelength of 330 nm. Two emission bands are apparently observed in PL spectra of the undoped and Cu-doped ZnO thin films: one is blue luminescence centering at 491 nm, and the other is deep level-green luminescence at 521 nm, which correspond to excitonic emission. The concentration of the $Cu^{2+}$ ions is another factor which is necessary to be optimized. Just as Fig. 12 shows, PL intensity increased with increasing of $Cu^{2+}$ concentration and reached a maximum at $0.45\times10^{-4}$ at % Cu doped ZnO. Increasing of the dopant content would rationally increase the number of dopant-related states in the band gap and subsequent enhancement of the recombination process through these states [36]. Nonetheless, addition of $Cu^{2+}$ dopant ions, more than the $0.45\times10^{-4}$ %, gives rise to appearance of concentration quenching effect due to non-radiative transitions between the neighboring dopant ions. Many researchers report this effect in transition metal-doped II-VI QDs [37-39].

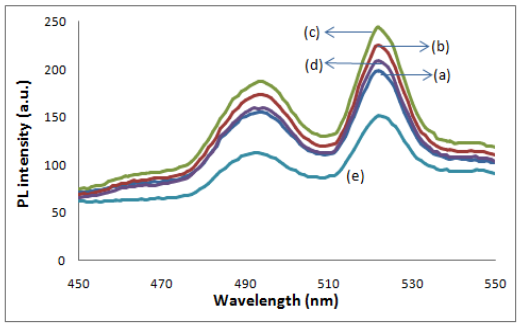


**Fig. 12.** PL spectra (a) pure ZnO and Cu doped ZnO prepared at different Cu concentrations (b) $0.5\times10^{-4}$, (c) $0.45\times10^{-4}$, (d) 0.03 and (e) 0.5.

Fig. 13 shows the PL spectra of ZnO:Cu thin films prepared at different temperatures and at 4 h deposition. The intensity of emission increases with increasing of temperature, which may be originate from the intrinsic defects such as oxygen vacancy [40] and oxygen interstitials [41]. Fig. 14 shows the PL spectra of ZnO:Cu thin films prepared at different deposition times and at 76 °C. The crystal lattice defects decrease with increasing deposition time and become more perfect in the nanocrystals. So, the photoluminescence peak intensities decreased with increasing deposition time.

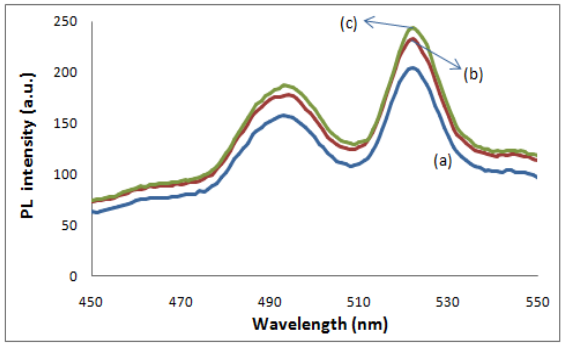


**Fig. 13** PL spectra of ZnO:Cu ($Cu=0.45\times10^{-4}$) thin films prepared at different temperatures (a) 56 °C, (b) 66 °C and (c) 76 °C for 4 h deposition.

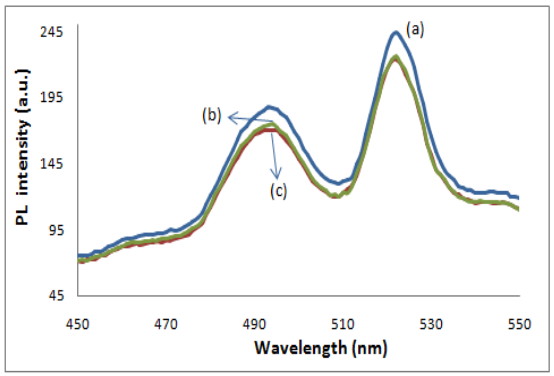


**Fig. 14.** PL spectra of ZnO:Cu ($Cu=0.45\times10^{-4}$) thin filmsprepared at temperature 76 °C and after different time (a) 4h (b) 6h (c) 8h.

**Table 2:** Band gap energy ( $E_g^{NC}$ ) values and nanocrystals radius (R) of the undoped and Cu-doped ZnO thin films

| Sample | deposition temperature (°C) | deposition times (h) | Cu doped (%) | $E_g^{NC}$ (eV) | R (nm) |
|---|---|---|---|---|---|
| ZnO | 60 | 3 | - | 3.96 | 1.75 |
| ZnO | 60 | 6 | - | 3.93 | 1.8 |
| ZnO | 60 | 8 | - | 3.91 | 1.83 |
| ZnO | 45 | 5 | - | 4.10 | 1.58 |
| ZnO | 60 | 5 | - | 4.00 | 1.7 |
| ZnO | 76 | 5 | - | 3.86 | 1.93 |
| ZnO | 76 | 2 | - | 3.97 | 1.74 |
| ZnO:Cu | 76 | 2 | $0.45\times10^{-4}$ | 3.94 | 1.79 |
| ZnO:Cu | 76 | 1.5 | $0.45\times10^{-4}$ | 4.05 | 1.63 |
| ZnO:Cu | 76 | 3 | $0.45\times10^{-4}$ | 3.91 | 1.83 |
| ZnO:Cu | 76 | 4 | $0.45\times10^{-4}$ | 3.70 | 2.35 |

*Elemental analysis*

Chemical composition of ZnS:Ni thin films were analyzed by ICP-AES and FTIR measurements. Table 3 shows the Cu/Zn atomic percent ratios for the ZnO:Cu films prepared at different Cu concentration and at 76 °C. ICP-AES analysis shows, with increasing in Cu precorsor, the Cu/Zn atomic ratios in the films increase. The co-deposition of ZnO and CuO quite difficult, because of the CuO (Ksp=$1\times10^{-19.7}$) is much less soluble than the ZnO (Ksp=$1\times10^{-16.7}$). Therefore, during the deposition process, the concentration of Cu precursor should be very lower than the concentration of Zn precursor. Hence, at very low amount of Cu precursor, ZnO can forms the main phase, whereas $Cu^{2+}$ ions are present as an impurity and can be incorporated gradually into the ZnO crystal lattice, depending on the concentration of Cu precursor.

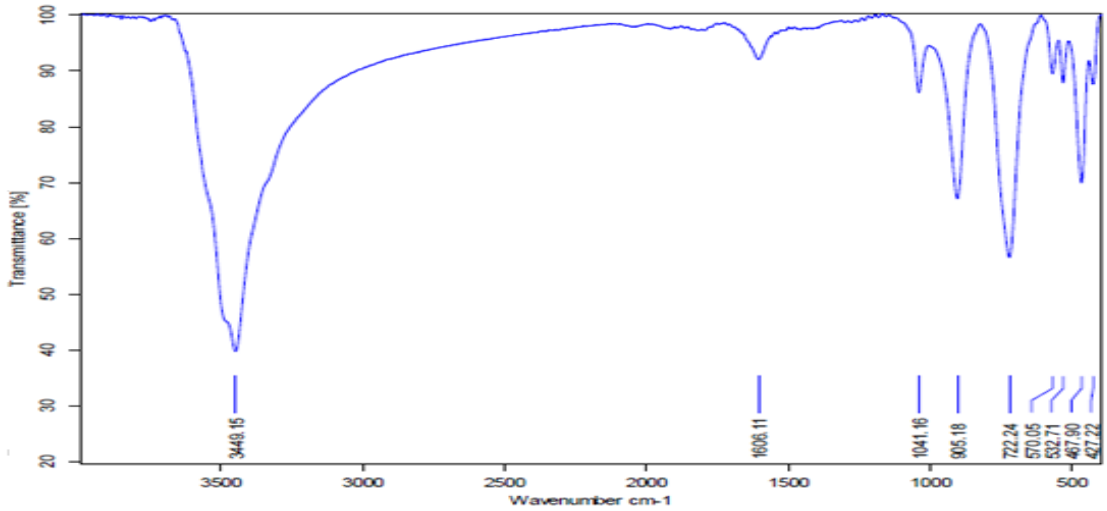


**Fig. 15.** FTIR spectra of ZnO:Cu thin films prepared at 76 °C for 8 h.

**Table 3:** The atomic ratio values of ZnO:Cu films prepared at 76 °C for 4 h.

| Cu doped (%) | Cu:Zn (%) |
|---|---|
| 0. $5\times10^{-5}$ | 0.041 |
| $0.45\times10^{-4}$ | 0.29 |
| $0.4\times10^{-4}$ | 0.55 |
| $0.4\times10^{-2}$ | 1.24 |
| 0.03 | 3.57 |

In order to investigate the presence of organic compounds as impurities in the ZnO:Cu thin films, the FTIR spectrum of films was obtained and studied. Fig. 15 shows the FTIR spectrum of ZnO:Cu thin films prepared at 76 °C for 8 h. The various vibration bonds of ZnO:Cu thin films were listed in Table 4. FTIR spectrum shows two main peaks in 427.22 and 532.71 $cm^{-1}$ which are attributed to ZnO and CuO bonds, respectively [42-44]. Some very weak peaks related to partial decomposition of $C_6H_{12}N_4$ molecules are observed in the films. Also, two peaks were observed in the FTIR spectrum, one very weak peak at 1606.11 $cm^{-1}$ and another broad peak at 3449.15 $cm^{-1}$ that must be related to the stretching and bending modes of trace amounts of adsorbed water on the film.

**Table 4:** The vibration bonds of the ZnO:Cu thin films

| Wavenumber ($cm^{-1}$) | bond |
|---|---|
| 3449.15 | OH |
| 1606.11 | OH |
| 1041.16 | C-N |
| 905.18 | C-H |
| 722.24 | C-C |
| 532.71 | CuO |
| 476.9 | $Zn(OH)_2$ |
| 427.22 | ZnO |

## CONCLUSIONS

Undoped and Cu-doped ZnO thin films have been prepared by chemical bath deposition method with potential applications in optoelectronics and solar cell engineering. The effect of Cu:Zn molar ,temperature and deposition time on the structural, optical and photoluminescence properties of the ZnO:Cu thin films were investigated. The XRD patterns and SEM images showed that the films consisted of small ZnO:Cu nanocrystals, showing quantum size effects. The green emission at 521 nm of the ZnO:Cu films can be related to the d–d optical transitions of $Cu^{2+}$ luminescent centers formed in the ZnO host crystals. Furthermore, with

increase in the Cu concentration, the PL emission intensity of the ZnO:Cu films is improved that can be attributed to the decrease of crystal defects density and also an enhancement in number of the radiation centers.

REFERENCES


1. B.K. Meyer, *Phys. Status Solidi B*, **241**, 231 (2004).
2. O. Madelung (ed), Data in Science and Technology: Semiconductors, Springer, Berlin, 1992.
3. S.H. Nam, M.H. Kim, D.G. Yoo, S.H. Jeong, D.Y. Kim, N.E. Lee, J.H. Boo., *Surf. Rev. Lett*, **1**, 121 (2010).
4. Y. Hamesa, Z. Alpaslan, A. Kosemen, S.E. San, Y. Yerli, *Sol. Energy*., **84**, 426 (2010).
5. R. Khan, H.W. Ra, J.T. Kim, W.S. Jang, D. Sharma, Y.H. Im, *Sens. Actuators B Chem*.,**150,** 389 (2010).
6. S. Singh, M.S.R. Rao, *Phys. Rev. B*, **80**, 045210 (2009).
7. S. Cho, J. Ma, Y. Kim, Y. Sun, *App. Phys. Lett.*, **75**, 2761 (1999).
8. D.M. Bagnall, Y.F. Chen, Z. Zhu, *Appl. Phys. Lett.*, **70**, 2230 (1997).
9. Z.K. Tang, G.K.L. Wong, P. Yu, *Appl. Phys. Lett.* **72**, 3270 (1998).
10. X.T. Zhang, Y.C. Liu, Z.Z. Zhi, *J. Lumin.*, **99**, 149 (2002).
11. S.M. Chung, S.H. Han, K.H. Son, *J. Lumin*., **114**, 227 (2005).
12. K. Vanheusden, W.L. Warren, C.H. Seager, D.R. Tallant, J.A. Voigt, B.E. Genade, *J. Appl. Phys.*,**79**, 7983 (1996).
13. P. Che, J. Meng, L. Guo, *J. Lumin*., **122**, 168 (2007).
14. Z.F. Liu, F.K. Shan, J.Y. Sohn, S.C. Kim, G.Y. Kim, Y.X. Li, Y.S. Yu, *J. Electroceram*. , **13**, 183 (2004).
15. D.J. Qiu, H.Z. Wu, A.M. Feng, Y.F. Lao, N.B. Chen, T.N. Xu, *Appl. Surf. Sci.*, **222**, 263 (2004).
16. F.K. Shan, B.I. Kim, G.X. Liu, Z.F. Liu, J.Y. Sohn, W.J. Lee, B.C Shin, Y.S. Yu, *J. Appl. Phys.*, **95,** 4772 (2004).
17. P. Dahany, V. Fleurovy, P. Thurianz, R. Heitzz, A. Hoffmannz, I. Broserz, *J. Phys.: Condens. Matter*., **10**, 2007 (1998).
18. A. Ohtomo, A. Tsukazaki, *Semicond. Sci. Technol.*, **20**, 1 (2005).
19. K. Ellmer, *J. Phys. D: Appl. Phys*., **33,** 17 (2000).
20. S. Fay, U. Kroll, C. Bucher, E.V. Sauvain, A. Shah, *Sol. Energy Mater. Sol. Cell*s, **86,** 385 (2005).
21. A. Drici, G. Djeteli, G. Tchangbedji, H. Derouiche, K. Jondo, K. Napo, J.C. Bernede, S.O. Djobo, M. Gbagba, *Phys. Status Solidi*, **201**, 1528 (2004).
22. A. Goudarzi, G. Motedayen Aval, R. Sahraei, H. Ahmadpoor, *Thin Solid Films*, **516**, 4953 (2008).
23. R. Sahraei, G. Motedayen Aval, A. Baghizadeh, M. Lamehi-Rachti, A. Goudarzi, M.H. Majles Ara, *Mater. Lett.*, **62**, 4345 (2008).
24. M. Wang, L. Zhang, *Mater. Lett.*, **63**, 301 (2009).
25. H. Mcmurdie, *Powder Diffraction*, **1**, 76 (1986).
26. J. Langford, D. Louer, *J. Appl. Crystalloger*., **24**, 149 (1991).
27. C. Suryanarayana, M. Grant Norton, X-Ray Diffraction A Practical Approach, Plenum Press. New York and London, 1998.
28. R. Sahraei, S. Noshadi, A. Goudarzi, *RSC Adv.*, **5**, 77354 (2015).
29. S. Major, A. Banerjee, K.L. Chopra, K.C. Nagpal, *Thin Solid Films*, **143**, 19 (1986).
30. L.E. Brus, *J. Chem. Physics*, **80**, 4403 (1984).
31. G. Hodes, S. Gorer, *J. Phys. Chem.*, **98**, 5338 (1994).
32. R. Sahraei, G. Motedayen Aval, A. Goudarzi, *J. Alloys Compd.*, **466**, 488 (2008).
33. S.J. Pearton, D.P. Norton, K. Ip, Y.W. Heo, T. Steiner, *Progress In Materials Science*, **50**, 293 (2005).
34. S. Adachi, Properties of Group-IV, III-V and II-VI Semiconductors, John Wiley and Sons, Ltd, West Sussex, England, 2005.
35. H. Hartnagel, A.L. Dawar, A.K. Jain, C. Jagadish, Semiconducting transparent thin films, Institute of Physics Publishing, Bristol and Philadelphia, 1995.
36. R. Sahraei, S. Darafarin, *Spectrochim. Acta Part A*, **149,** 941 (2015.
37. R. Sahraei, S. Darafarin, *J. Lumin.*, **149,** 170 (2014).
38. Y. Song, Y. Li, X. Wang, X. Su, Q. Ma, *RSC Adv.*, **5**, 6271 (2015).
39. S. Darafarin, R. Sahraei, A. Daneshfar, *J. Alloys Compd.*, **658**, 780 (2016).
40. K. Vanheusden, C.H. Seager, W.L. Warren, D.R. Tallant, J.A. Voigt, *Appl. Phys. Lett.*, **68**, 403 (1996).
41. S.A. Studenikin, N. Golego, M. Cocivera, *J. Appl. Phys.*, **84**, 2287 (1998).
42. J.R. Ferraro, Low-Frequency Vibrations of Inorganic and Coordination Compounds, Plenum, New York, 1971.
43. R. Sahraei, A. Daneshfar, A. Goudarzi, S. Abbasi, M.H. Majles Ara, F. Rahimi, *J. Mater. Sci.: Mater. Electron.*, **24**, 260 (2013).
44. M.R. Johan, M.S. MohdSuan, N.L. Hawari, H.A. Ching, *Int. J. Electrochem. Sci.*, **6**, 6094 (2011).